Effect of the interference between interband currents on the crystal harmonic spectra

Yue Qiao [1,2] Jiaqi Chen,[3] Yanqiu Huo,[4] Huaqiu Liang,[4] Ruixian Yu,[1,2] Jigen Chen [4,*] Wenjun Liu,[5,†]
Shicheng Jiang [6,‡] and Yujun Yang [1,2,§]

[1]*Institute of Atomic and Molecular Physics, Jilin University, Changchun 130012, China*
[2]*Jilin Provincial Key Laboratory of Applied Atomic and Molecular Spectroscopy (Jilin University), Changchun 130012, China*
[3]*School of Materials Science and Engineering, Taizhou University, Jiaojiang 318000, Zhejiang, China*
[4]*Zhejiang Provincial Key Laboratory for Cutting Tools, Taizhou University, Jiaojiang 318000, Zhejiang, China*
[5]*State Key Laboratory of Information Photonics and Optical Communications, School of Science, P. O. Box 91,*
Beijing University of Posts and Telecommunications, Beijing 100876, China
[6]*State Key Laboratory of Precision Spectroscopy, East China Normal University, Shanghai 200062, China*

By numerically solving the semiconductor Bloch equation, we study the high-order harmonic emission spectrum of a MgO crystal under the interaction of a linearly polarized laser pulse. Based on two-band and three-band models, by comparing the variation of the harmonic spectrum with the laser peak intensity, it is found that when the laser intensity is lower, the harmonic spectra from both cases are generally consistent above the minimum band gap. However, some harmonic intensities in the three-band model are significantly enhanced or weakened compared to the two-band case when the laser intensity is higher. By analysis of the electron population and the harmonic phase, it is demonstrated that the harmonic enhancement or reduction is caused by the interference between two interband polarization sources, one of which originates from the current between the first conduction band and the valence band and the other of which is from the polarization between the second and the first conduction band. The harmonic interference between different interband currents contains rich dynamic information and has a significant impact on the harmonic structure and yield, which is helpful for further understanding the generation mechanism of crystal harmonics.

I. INTRODUCTION

High-order harmonic generation (HHG) can be observed when an intense laser field interacts with atoms, molecules, and solids [1–6]. High-order harmonic generation is an important coherent light source in extreme ultraviolet and even soft-x-ray bands [7]. Due to the large bandwidth of its emission spectrum, HHG is one of the main means to produce attosecond (10^{-18} s) pulses [8–13]. High-order harmonic generation is generated by the recollision of ionized electrons, which carries structural characteristics of the material and is applied to the detection of the material structure and ultrafast electron dynamics [14–26].

Gaseous HHG was first observed in [27,28] and HHG was extended to solids in [3]. Ndabashimiye *et al.* compared the HHG from Ar and Kr in solid and gas phases. They found that the harmonic spectra from rare-gas solids exhibit multiple platforms, which are far beyond the atomic limit of the corresponding gas-phase harmonics measured under similar conditions [29]. The rare-gas solid is a bridge connecting the atomic and solid HHG, which has important reference signif-

icance for studying the HHG mechanism of a solid and gas. Crystals have high electronic density and periodic structures. Thus it is expected to generate harmonic signals with higher intensity compared to the gaseous targets [30,31]. Therefore, solid HHG has attracted increasing attention [32–42].

The generation mechanism of solid HHG can be given by the framework of energy band theory [43]. In the frame of band theory, HHG in crystals mainly includes four sources: (i) intraband current produced by the oscillatory motion of electrons (holes) in the conduction band (valence band), (ii) interband polarization from the electronic transition between two energy bands, (iii) Berry curvature, which can induce the anomalous transverse intraband current, and harmonic photons, which will be generated in the direction perpendicular to the polarization of the laser field [44], and (iv) mixture terms [45,46]. Recent studies have shown that the HHG generated by these mechanisms has different characteristics which influence each other. Vampa *et al.* found that contributions of intraband and interband harmonics have significantly different dependences on the driving laser wavelength [47]. Through the time-frequency analysis, Wu *et al.* proved that radiation mechanisms of intraband and interband harmonics are very different in the dynamic process [48]. Wang *et al.* studied the interference effect between interband and intraband currents in the HHG of the ZnO crystal [49]. They found that when interband and intraband currents have good synchronization, the constructive interference contribution of interband and

*kiddchen@126.com
†jungliu@bupt.edu.cn
‡scjiang@lps.ecnu.edu.cn
§yangyj@jlu.edu.cn

intraband currents dominates the harmonic spectrum. When they lose synchronization, the destructive interference cancels out some of the contributions from interband and intraband currents. Zhao *et al.* checked the effect of the interband polarization on harmonics below the minimum band gap of the MgO crystal [50]; with the increase of the incident laser intensity, the electronic transition between two conduction bands has an important contribution to the harmonics just below the band gap, and the coherent interference of the intraband current and the interband polarization leads to harmonic enhancement.

The above studies focus on the interference between the two harmonic emission mechanisms of the crystal, that is, the interference between intraband harmonics and interband harmonics. For crystals with multiple energy bands, whether different interband harmonics and their behaviors can be observed in the harmonic spectrum still needs to be studied further. Uzan *et al.* experimentally proved that multiple energy bands are the reason for the enhancement in the yield of different harmonic regions in MgO [16]. Uzan-Narovlansky *et al.* studied the dynamic transitions between different bands of MgO crystals and discussed their structural dependence. It was shown that the imprint of the transitions between the adjacent conduction bands on the harmonic emission can be used to observe light-induced modifications of the bands [17]. Du *et al.* showed that when multiple energy bands were considered, multiple emission channels in the solid can extend the cutoff energy of the platform in the harmonic spectra and enhance intraband and interband contributions. The interference of different channels makes the harmonic spectral structure more complex [51]. The work of Xia *et al.* demonstrated that

the interband current between higher conduction bands has a great influence on the harmonic emission when the population in the higher conduction band is larger, and the structure of the second plateau can be affected by the action of different paths [52]. Although these investigations do not explore the interference process of the interband harmonics between different bands in detail, their results testify that the contribution of higher conduction bands cannot be ignored under certain conditions.

In this work, the MgO crystal in the Γ-X direction is irradiated by a linearly polarized laser pulse. Based on two-band and three-band models, solid harmonic spectra above the minimum band gap are systematically studied. It is found that under certain laser conditions, compared with the two-band case, the intensity of the harmonic with the specific energy can be obviously enhanced or weakened in the three-band model. Through the analysis of the electron population on the conduction band and the harmonic phase, we prove that this harmonic enhancement or weakening phenomenon originates from the interference between interband harmonics generated by the first conduction band with the valence band and the interband HHG by the second conduction band with the first conduction one.

II. SCHEME AND THEORETICAL METHOD

In this work, semiconductor Bloch equations (SBEs) [46,47,53–55] are adopted to study the high-order harmonic emission from the MgO crystal in the laser pulse. The three-band SBEs are shown as (atomic units are used throughout this paper unless specified otherwise)

$$\frac{\partial}{\partial t} P_k^{vc_1} = -i\left([\varepsilon_{c_1}(k) - \varepsilon_v(k)] - \frac{i}{T_2} \right) P_k^{vc_1} - i\left(1 - f_k^{c_1} - f_k^v\right) d_{c_1v}(k) E(t) + E(t) \nabla_k P_k^{vc_1} + iE(t)\left[d_{c_2v}(k) P_k^{c_2c_1} - d_{c_1c_2}(k) P_k^{vc_2} \right], \tag{1}$$

$$\frac{\partial}{\partial t} P_k^{vc_2} = -i\left([\varepsilon_{c_2}(k) - \varepsilon_v(k)] - \frac{i}{T_2} \right) P_k^{vc_2} - i\left(1 - f_k^{c_2} - f_k^v\right) d_{c_2v}(k) E(t) + E(t) \nabla_k P_k^{vc_2} + iE(t)\left[d_{c_1v}(k) P_k^{c_1c_2} - d_{c_2c_1}(k) P_k^{vc_1} \right], \tag{2}$$

$$\frac{\partial}{\partial t} P_k^{c_1c_2} = -i\left([\varepsilon_{c_2}(k) - \varepsilon_{c_1}(k)] - \frac{i}{T_2} \right) P_k^{c_1c_2} + i\left(f_k^{c_2} - f_k^{c_1}\right) d_{c_2c_1}(k) E(t) + E(t) \nabla_k P_k^{c_1c_2} + iE(t)\left[d_{vc_1}(k) P_k^{vc_2} - d_{c_2v}(k) P_k^{vc_1^*} \right], \tag{3}$$

$$\frac{\partial}{\partial t} f_k^v = 2\,\mathrm{Im}\left[d_{c_1v}(k) E(t) P_k^{vc_1^*} + d_{c_2v}(k) E(t) P_k^{vc_2^*} \right] + E(t) \nabla_k f_k^v, \tag{4}$$

$$\frac{\partial}{\partial t} f_k^{c_1} = 2\,\mathrm{Im}\left[d_{c_1c_2}(k) E(t) P_k^{c_2c_1^*} + d_{c_1v}(k) E(t) P_k^{vc_1^*} \right] + E(t) \nabla_k f_k^{c_1}, \tag{5}$$

$$\frac{\partial}{\partial t} f_k^{c_2} = 2\,\mathrm{Im}\left[d_{c_2c_1}(k) E(t) P_k^{c_1c_2^*} + d_{c_2v}(k) E(t) P_k^{vc_2^*} \right] + E(t) \nabla_k f_k^{c_2}. \tag{6}$$

Here $\varepsilon_\lambda(k)$ ($\lambda = v, c_1, c_2$) represents the energy of the valence band and the first and second conduction bands, respectively; f_k^λ ($\lambda = v, c_1, c_2$) is the hole density in the valence band and the electronic population in the first and second conduction bands, respectively; and $P_k^{\lambda_1\lambda_2}$ ($\lambda_1\lambda_2 = vc_1, vc_2, c_1c_1$) and $d_{\lambda_1\lambda_2}(k)$ are micropolarizations and transition dipole moments (TDMs) between different energy bands, respectively.

Following the methods in Ref. [56], the band structure and smoothed TDMs of the MgO crystal in the Γ-X direction are shown in Fig. 1. The form of the laser pulse used in this work is $E(t) = \sqrt{I} f(t) \cos(\omega t)$. The envelope function $f(t)$ is the trapezoidal envelope with a one-cycle linear turn-on and a one-cycle linear turnoff. The dephasing time T_2 has been set to about a quarter of an optical period. The total intraband
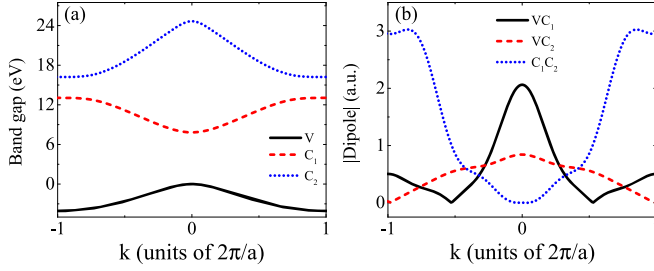
FIG. 1. (a) Band structure of MgO in the Γ-X direction and (b) k-dependent transition dipole moments.

FIG. 2. Harmonic spectra as a function of the laser peak intensity: (a) two-band model and (b) three-band case.

current $J_{\text{intra}}(t)$ is

$$J_{\text{intra}}(t) = \sum_{\lambda=c_1,c_2,v} \int_{\text{BZ}} v_\lambda(k) f_k^\lambda dk. \tag{7}$$

Here BZ represents the Brillouin zone and $v_\lambda(k) = \nabla_k E(k)$ is the group velocity. The total interband current $J_{\text{inter}}(t)$ and interband currents between different bands can be calculated as

$$J_{\text{inter}}(t) = \sum_{\lambda_1\lambda_2} \frac{\partial}{\partial t} \int_{\text{BZ}} d_{\lambda_1\lambda_2}(k) P_k^{\lambda_1\lambda_2} dk + \text{c.c.}, \tag{8}$$

$$J_{vc_1}(t) = \frac{\partial}{\partial t} \int_{\text{BZ}} d_{vc_1}(k) P_k^{vc_1} dk + \text{c.c.}, \tag{9}$$

$$J_{vc_2}(t) = \frac{\partial}{\partial t} \int_{\text{BZ}} d_{vc_2}(k) P_k^{vc_2} dk + \text{c.c.}, \tag{10}$$

$$J_{c_1c_2}(t) = \frac{\partial}{\partial t} \int_{\text{BZ}} d_{c_1c_2}(k) P_k^{c_1c_2} dk + \text{c.c.} \tag{11}$$

Finally, the harmonic spectrum can be obtained by the Fourier transform of the current. The total harmonic $S_{\text{total}}(\omega)$, total interband harmonic $S_{\text{inter}}(\omega)$, the interband harmonic between the valence band and the first conduction band $S_{vc_1}(\omega)$, the interband harmonic between the valence band and the second conduction band $S_{vc_2}(\omega)$, and the interband harmonic between the first conduction band and the second conduction band $S_{c_1c_2}(\omega)$ are given as

$$S_{\text{total}}(\omega) \propto \left| \int_{-\infty}^{\infty} [J_{\text{inter}}(t) + J_{\text{intra}}(t)] e^{iwt} dt \right|^2, \tag{12}$$

$$S_{\text{inter}}(\omega) \propto \left| \int_{-\infty}^{\infty} [J_{\text{inter}}(t)] e^{iwt} dt \right|^2, \tag{13}$$

$$S_{vc_1}(\omega) \propto \left| \int_{-\infty}^{\infty} [J_{vc_1}(t)] e^{iwt} dt \right|^2, \tag{14}$$

$$S_{vc_2}(\omega) \propto \left| \int_{-\infty}^{\infty} [J_{vc_2}(t)] e^{iwt} dt \right|^2, \tag{15}$$

$$S_{c_1c_2}(\omega) \propto \left| \int_{-\infty}^{\infty} [J_{c_1c_2}(t)] e^{iwt} dt \right|^2. \tag{16}$$

III. RESULTS AND DISCUSSION

In Fig. 2 we show the variation of the total harmonic intensity with the laser peak intensity for the two-band and three-band models. The selected laser wavelength is 1500 nm and the laser duration is seven optical cycles. As can be seen from the figure, with the increase of the laser peak intensity,
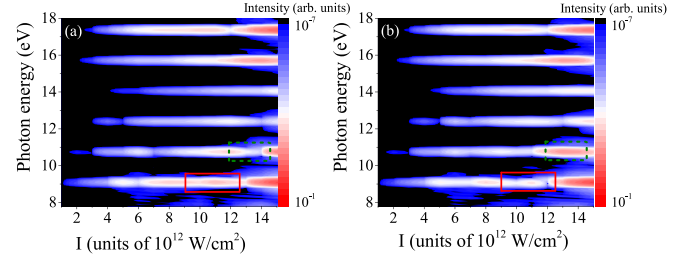
the overall harmonics gradually become stronger. The two-band and three-band harmonic spectra all have a minimum near 14 eV. When the laser intensity is lower, the harmonic intensities for the two-band and three-band models are basically the same. With the enhancement of the driving laser intensity, it can be found that the three-band and two-band harmonics have obvious differences at specific energies. When the laser intensity range is about (12×10^{12})–(14.5×10^{12}) W/cm^2, the harmonic with an energy of 10.8 eV (corresponding to the 13th) in the three-band model is significantly stronger than that in the two-band model, which is marked by the green dotted line in Fig. 2. When the laser intensity range is around (9×10^{12})–(12.5×10^{12}) W/cm^2, the harmonic with the energy 9.1 eV (corresponding to the 11th) in the three-band model is significantly weaker than that in the two-band model, which is presented by the red solid line in the figure.

To explain the intensity difference between the harmonic spectra for the two-band and three-band models at the specific energies, we first analyze the band gap of the MgO crystal in the Γ-X direction, as shown in Fig. 3. It can be observed that the band gap between the valence band and the first conduction band (VC_1) is about 7.8–17.8 eV. The band gap between the valence band and the second conduction band (VC_2) is about 20.5–24.5 eV and the band gap between two conduction bands (C_1C_2) is about 3.2–16.8 eV. The band gaps of VC_1 and C_1C_2 overlap at energies around 7.8–16.8 eV [$k \in (-0.5)$–0 and $k \in 0$–0.5], so the harmonic emission from VC_1 and C_1C_2 has the opportunity to interfere. More importantly, in the range of the band-gap reduplication, there is a case where the TDM
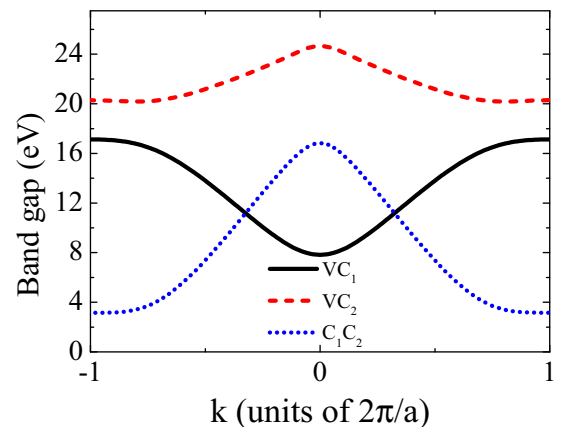

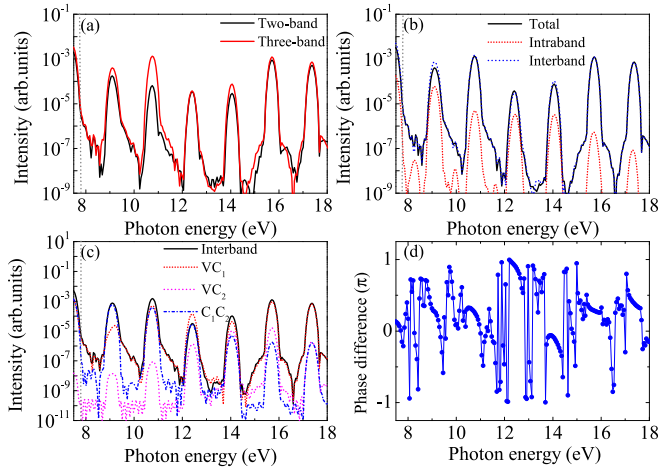FIG. 3. Band gap of MgO in the Γ-X direction.

FIG. 4. (a) Total harmonic spectra calculated by two-band (black solid line) and three-band models (red solid line). (b) Total harmonic spectrum (black solid line) and harmonic spectra generated by interband currents (blue dashed line) and intraband currents (red dotted line) from the three-band model. (c) Total interband harmonic spectrum (black solid line), harmonic spectrum from the interband current between VC_1 (red dotted line), harmonic spectrum from the polarization between VC_2 (pink dashed line), and harmonic spectrum from the interband current between C_1C_2 (blue dash-dotted line). (d) Phase difference between the harmonics of VC_1 and the harmonics of C_1C_2. The laser peak intensity is 13×10^{12} W/cm^2 and the other parameters are the same as in Fig. 2.

FIG. 5. Same as in Fig. 4 but the laser intensity is 11.7×10^{12} W/cm^2.

magnitude of C_1C_2 is comparable to that of VC_1, or even larger than the TDM magnitude of VC_1 [$k \in (-0.5)$–(-0.3) and $k \in 0.3$–0.5], and the energy range is about 7.8–12 eV, as shown in Fig. 1(b). According to the inversion symmetry of the MgO crystal, it can only emit odd harmonics when the crystal is driven by the long linearly polarized laser pulse. In the region of 7.8–12 eV, it can emit harmonics with an energy of 9.1 eV (corresponding to the 11th) and an energy of 10.8 eV (corresponding to the 13th) when the laser wavelength is 1500 nm, which is consistent with the energy position where one can find the harmonic intensity difference between two-band and three-band cases in Fig. 2. Since the harmonic intensity is strongly related to the TDM magnitude, this means that C_1C_2 has the opportunity to produce harmonic emission with an intensity close to that from VC_1, which in turn interferes with the overall harmonic process.

To examine this interference mechanism, the harmonic spectra from the three-band and two-band models are exhibited in Fig. 4(a) when the laser peak intensity is 13×10^{12} W/cm^2. The gray dotted line in the figure marks the position of the minimum band gap between VC_1. We can see that the 10.8 eV harmonic intensity in the case of the three-band model is much higher than that for the two-band model. Figure 4(b) shows the total harmonic (black solid line), the intraband harmonic (red dotted line), and the interband harmonic (blue dashed line) for the three-band model. It can be noticed that the total harmonics with an energy higher than the minimum band gap between VC_1 are mainly dominated by interband currents. Since the energy position of the harmonic enhancement is mainly dominated by interband harmonics, we divided
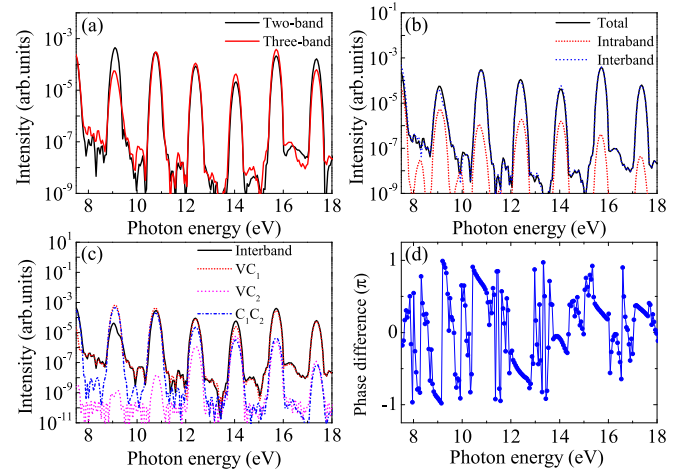
the total interband harmonics into the harmonic spectra between different energy bands, as presented in Fig. 4(c). It can be found that when the harmonic energy is 10.8 eV, the intensity of the harmonic between VC_1 is close to that of C_1C_2. In the following, we further analyze the harmonic phase. Figure 4(d) gives the phase difference between the harmonics of VC_1 and the harmonics of C_1C_2. It can be seen that the harmonic phase difference is close to 0 near an energy of 10.8 eV, which satisfies the condition of the constructive interference. Therefore, when the laser intensity is 13×10^{12} W/cm^2, the intensity of the harmonic with an energy of 10.8 eV in the case of the three-band model will be higher than that of the two-band model.

After analyzing the phenomenon of harmonic coherence enhancement, we further discuss the phenomenon of harmonic coherence weakening. Figure 5(a) shows the harmonic spectra of the three-band and two-band models when the laser peak intensity is 11.7×10^{12} W/cm^2. One can see that in the case of the three-band model, the intensity of the harmonic with the energy at 9.1 eV is much weaker than that for the two-band model. Figure 5(b) shows the total harmonic (black solid line), the intraband harmonic (red dotted line), and the interband harmonic (blue dashed line) for the three-band model. It can be observed that at this laser intensity, the interband harmonics also play a major role in the total harmonics when the energy is higher than the minimum band gap between VC_1. The energy position of the harmonic weakening is also dominated by interband currents. Similarly, the total interband harmonics are separated in Fig. 5(c), which presents the harmonic spectra between different energy bands. It can be seen that when the harmonic energy is 9.1 eV, the harmonic intensity between VC_1 is close to that of C_1C_2. By further considering the phase difference between the harmonics of VC_1 and the harmonics of C_1C_2, we find that the harmonic phase difference is close to $-\pi$ near an energy of 9.1 eV, which satisfies the condition of destructive interference, as displayed in Fig. 5(d). This result confirms that the intensity of the 9.1 eV harmonic from the three-band model is weaker than that in the two-band case when the incident laser peak intensity is 11.7×10^{12} W/cm^2.
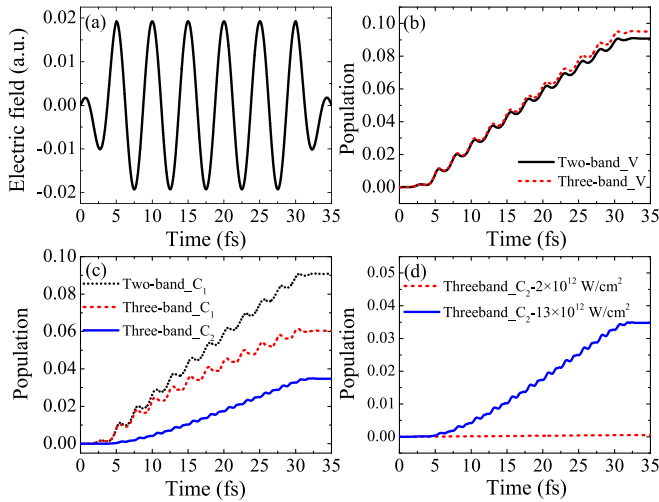
FIG. 6. (a) Laser field when the laser peak intensity is 13×10^{12} W/cm^2. (b) Hole population in the valence band. (c) Electron population in the first conduction band from two-band and three-band cases and the electron population in the second conduction from the three-band model. (d) Electron population in the second conduction band when the laser peak intensities are 2×10^{12} and 13×10^{12} W/cm^2.

To understand the change in interband harmonic interference effects with the laser intensity, we analyze the time evolution of the electron population at each energy band for different model simulations, as shown in Fig. 6. Figure 6(a) is the laser electric field when the driving laser peak intensity is 13×10^{12} W/cm^2 and the other laser parameters are consistent with Fig. 2. Under the action of the laser electric field, hole populations of the valence band from the two-band (black solid line) and three-band models (red dotted line) gradually increase with time and the hole populations in both cases are almost the same, as displayed in Fig. 6(b). It can be observed from Fig. 6(c) that the electronic population of the first conduction band from the two-band model increases with time and the electronic population of the first conduction band in the three-band case is weaker than that in the two-band model. This is because some electrons in the first conduction band transition to the second conduction band. From the blue solid line in Fig. 6(c) it can be seen that the electron population on the second conduction band gradually increases with time. At the end of the laser pulse, the electron population on the second conduction band is close to 4%. In Fig. 6(d) we also show a comparison of the electronic populations on the second conduction at a lower intensity of 2×10^{12} W/cm^2 and a higher intensity of 13×10^{12} W/cm^2. It can be seen that the increase in the laser peak intensity enhances the electronic population and the proportion of the second conduction band. Therefore, at higher laser intensities, the second conduction band will have a greater impact on the harmonic emission and it is possible to observe the difference of the HHG spectra between two-band and three-band models.

In addition, we also observed the interference effects at other laser wavelengths; these results are given in the Appendix. Our research is based on the fact that the band gap of VC$_1$ and C$_1$C$_2$ in MgO crystal in the Γ-X direction has energy

overlap, and the TDM magnitude of C$_1$C$_2$ is comparable to that of VC$_1$ in this energy overlap range. We believe that the interference phenomenon of the interband HHG can be observed in crystal materials satisfying the above two conditions.

IV. CONCLUSION

By modeling the interaction between the MgO crystal and the linearly polarized laser pulse, it was found that the harmonic spectra of the two-band and three-band models above the minimum band gap are significantly different at the higher driving laser peak intensity. Through the analysis of the time-dependent electronic population, it was confirmed that the electron population of the second conduction band is greatly enhanced with an increase of the driving laser intensity, which in turn enhances the contributions from the polarization between C$_1$C$_2$ at the specific energy. The corresponding harmonic intensity from the polarization between C$_1$C$_2$ can even be close to that from the interband current between VC$_1$. The difference in the harmonic emission spectra of the two-band and three-band models can be attributed to the constructive or destructive interference between the harmonics from VC$_1$ and those from C$_1$C$_2$. This result reveals the interference mechanism of different interband harmonics and deepens the understanding of the electronic dynamic behavior of solids in the strong laser pulse. By adjusting incident laser parameters, coherent characteristics of the interband harmonic spectra can be used to control specific order harmonics. As shown in Refs. [57,58], the laser pulse chirp plays an important role in the phase of the generated harmonic and thus could affect interference effect. A detailed study of the influence of the laser chirp on the solid HHG is left for future work.

APPENDIX: RESULTS AT OTHER LASER WAVELENGTHS

In this Appendix we study the interference effects at laser wavelengths of 1300 and 1600 nm. Figures 7(a) and 7(b) present the variation of the total harmonic spectra with the laser peak intensity for the two-band and three-band models, respectively, at a wavelength of 1300 nm. It can be seen that when the laser intensity range is about (10×10^{12})–(16.5×10^{12}) W/cm^2, the harmonic with an energy of 10.5 eV (corre-

FIG. 7. Harmonic spectra as a function of the laser peak intensity when the laser wavelength is 1300 nm: (a) two-band model and (b) three-band case. (c) Total interband harmonic spectrum (black solid line), harmonic spectrum from the interband current between VC_1 (red dotted line), harmonic spectrum from the polarization between VC_2 (pink dashed line), and harmonic spectrum from the interband current between C_1C_2 (blue dash-dotted line) when the laser peak intensity is 16×10^{12} W/cm^2. (d) Phase difference between the harmonics of VC_1 and the harmonics of C_1C_2 when the laser peak intensity is 16×10^{12} W/cm^2. (e) and (f) Same as (c) and (d), respectively, but the laser intensity is 14×10^{12} W/cm^2.
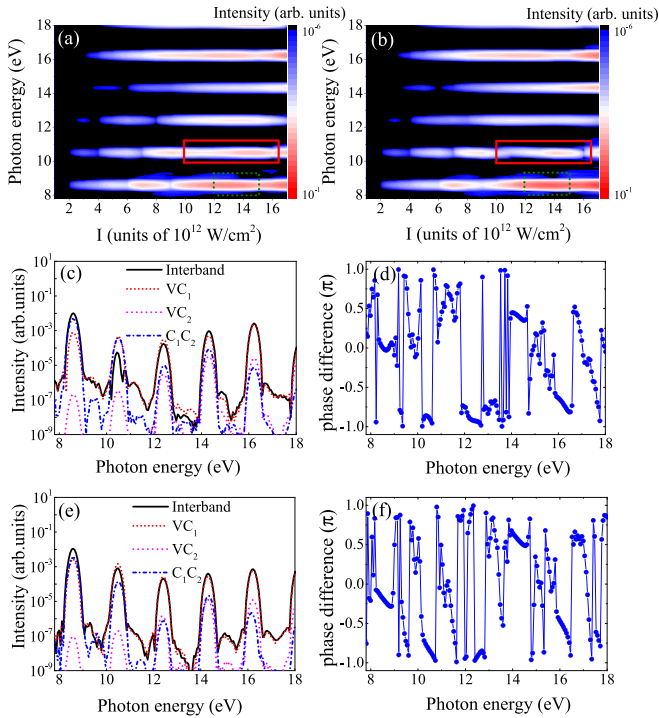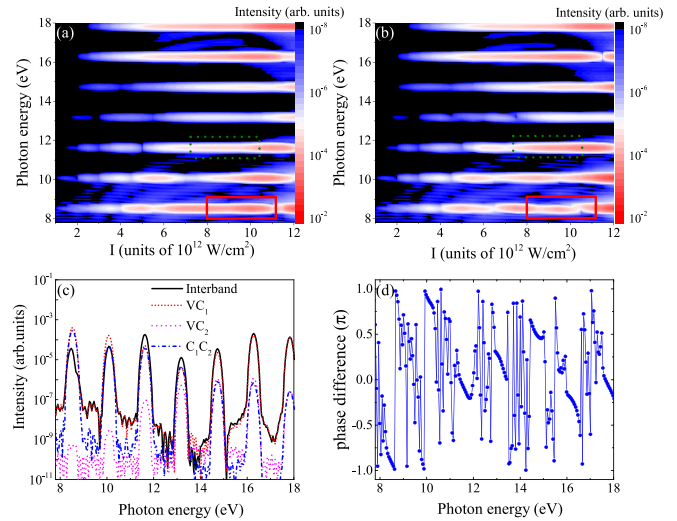
FIG. 8. Harmonic spectra as a function of the laser peak intensity when the laser wavelength is 1600 nm: (a) two-band model and (b) three-band case. (c) Total interband harmonic spectrum (black solid line), harmonic spectrum from the interband current between VC_1 (red dotted line), harmonic spectrum from the polarization between VC_2 (pink dashed line), and harmonic spectrum from the interband current between C_1C_2 (blue dash-dotted line) when the laser peak intensity is 10×10^{12} W/cm^2. (d) Phase difference between the harmonics of VC_1 and the harmonics of C_1C_2 when the laser peak intensity is 10×10^{12} W/cm^2.

sponding to the 11th) in the three-band model is significantly weaker than that in the two-band model, which is marked by the red solid line in the figure. When the laser intensity range is about (12×10^{12})–(15×10^{12}) W/cm^2, the harmonic with an energy of 8.6 eV (corresponding to the ninth) in the three-band model is stronger than that in the two-band model, which is marked by the green dotted line in the figure. Figure 7(c) shows the harmonic spectra between different bands in the three-band model when the wavelength is 1300 nm and the laser intensity is 16×10^{12} W/cm^2. It can be found that when the harmonic energy is 10.5 eV, the intensity of the harmonic between VC_1 is close to that of C_1C_2. Figure 7(d) gives the phase difference between the harmonics of VC_1 and the harmonics of C_1C_2; we notice that the harmonic phase difference is close to $-\pi$ near an energy of 10.5 eV, which satisfies the condition of destructive interference. Therefore, when the laser intensity is 16×10^{12} W/cm^2, the efficiency of the harmonic with an energy of 10.5 eV in the case of the three-band model is weaker than that of the two-band model. Figure 7(e) presents the harmonic spectra between different bands in the three-band model when the wavelength is 1300 nm and the laser intensity is 14×10^{12} W/cm^2. It can be found that when the harmonic energy is 8.6 eV, the intensity of

the harmonic between VC_1 is close to that of C_1C_2. Figure 7(f) gives the phase difference between the harmonics of VC_1 and the harmonics of C_1C_2; one can observe that the harmonic phase difference is close to 0 near an energy of 8.6 eV, which satisfies the condition of constructive interference. Therefore, when the laser intensity is 14×10^{12} W/cm^2, the efficiency of the harmonic with an energy of 8.6 eV in the case of the three-band model is stronger than that of the two-band model. According to the above results, the effect of interband harmonic interference still exists when the laser wavelength is 1300 nm.

We further simulated the variation of the harmonic spectrum with the laser intensity at a wavelength of 1600 nm under the two-band and three-band conditions, as shown in Figs. 8(a) and 8(b), respectively. It can be seen that when the laser intensity range is about (8×10^{12})–(11×10^{12}) W/cm^2, the harmonic with an energy of 8.5 eV (corresponding to the 11th) in the three-band model is significantly weaker than that in the two-band case, which is marked by the red solid line in the figure. When the laser intensity range is about (7.5×10^{12})–(10.5×10^{12}) W/cm^2, the harmonic with an energy of 11.6 eV (corresponding to the 15th) in the three-band model is stronger than that in the two-band case, which is marked by the green dotted line in the figure. Figure 8(c) shows the harmonic spectra between different bands in the three-band model when the wavelength is 1600 nm and the laser intensity is 10×10^{12} W/cm^2. It can be found that when the harmonic energies are 8.5 and 11.6 eV, the intensity of the harmonic between VC_1 is close to that of C_1C_2. Figure 8(d) gives the phase difference between the harmonics of VC_1 and the harmonics of C_1C_2; we see that the harmonic phase differ-

ence is close to $-\pi$ near an energy of 8.5 eV, which satisfies the condition of destructive interference. The harmonic phase difference is close to 0 near an energy of 11.6 eV, which satisfies the condition of constructive interference. Therefore, when the laser intensity is 10×10^{12} W/cm^2, the efficiency of the harmonic with an energy of 8.5 eV in the case of the

three-band model is weaker than that of the two-band model and the intensity of the harmonic with an energy of 11.6 eV in the case of the three-band model is stronger than that of the two-band model. In summary, the interference phenomenon of the interband harmonic can be observed in a wide wavelength range.

[1] P. B. Corkum, Phys. Rev. Lett. **71**, 1994 (1993).

[2] M. Lewenstein, P. Balcou, M. Y. Ivanov, A. L'Huillier, and P. B. Corkum, Phys. Rev. A **49**, 2117 (1994).

[3] S. Ghimire, A. D. DiChiara, E. Sistrunk, P. Agostini, L. F. DiMauro, and D. A. Reis, Nat. Phys. **7**, 138 (2011).

[4] G. Vampa, T. J. Hammond, N. Thiré, B. E. Schmidt, F. Légaré, C. R. McDonald, T. Brabecand, and P. B. Corkum, Nature (London) **522**, 462 (2015).

[5] E. Goulielmakis and T. Brabec, Nat. Photon. **16**, 411 (2022).

[6] Y. Lang, Z. Peng, J. Liu, Z. Zhao, and S. Ghimire, Phys. Rev. Lett. **129**, 167402 (2022).

[7] Z. Chang, A. Rundquist, H. Wang, M. M. Murnane, and H. C. Kapteyn, Phys. Rev. Lett. **79**, 2967 (1997).

[8] P. M. Paul, E. S. Toma, P. Breger, G. Mullot, F. Augé, P. Balcou, H. G. Muller, and P. Agostini, Science **292**, 1689 (2001).

[9] P. Antoine, A. L'Huillier, and M. Lewenstein, Phys. Rev. Lett. **77**, 1234 (1996).

[10] F. Krausz and M. Ivanov, Rev. Mod. Phys. **81**, 163 (2009).

[11] Z. Nourbakhsh, N. Tancogne-Dejean, H. Merdji, and A. Rubio, Phys. Rev. Appl. **15**, 014013 (2021).

[12] X. Zhao, S.-J. Wang, W.-W. Yu, H. Wei, C. Wei, B. Wang, J. Chen, and C. D. Lin, Phys. Rev. Appl. **13**, 034043 (2020).

[13] S.-S. Zhou, W.-D. Lan, J.-G. Chen, J. Wang, F.-M. Guo, and Y.-J. Yang, Phys. Rev. A **106**, 023510 (2022).

[14] G. Vampa, T. J. Hammond, N. Thiré, B. E. Schmidt, F. Légaré, C. R. McDonald, T. Brabec, D. D. Klug, and P. B. Corkum, Phys. Rev. Lett. **115**, 193603 (2015).

[15] J. B. Bertrand, H. J. Wörner, P. Hockett, D. M. Villeneuve, and P. B. Corkum, Phys. Rev. Lett. **109**, 143001 (2012).

[16] A. J. Uzan, G. Orenstein, Á. Jiménez-Galán, C. McDonald, R. E. F. Silva, B. D. Bruner, N. D. Klimkin, V. Blanchet, T. Arusi-Parpar, M. Krüger, A. N. Rubtsov, O. Smirnova, M. Ivanov, B. Yan, T. Brabec, and N. Dudovich, Nat. Photon. **14**, 183 (2020).

[17] A. J. Uzan-Narovlansky, Á Jiménez-Galán, G. Orenstein, R. E. F. Silva, T. Arusi-Parpar, S. Shames, B. D. Bruner, B. Yan, O. Smirnova, M. Ivanov, and N. Dudovich, Nat. Photon. **16**, 428 (2022).

[18] H. Lakhotia, H. Y. Kim, M. Zhan, S. Hu, S. Meng, and E. Goulielmakis, Nature (London) **583**, 55 (2020).

[19] J. Chen, Q. Xia, and L. Fu, Phys. Rev. A **104**, 063109 (2021).

[20] L. Li, P. Lan, L. He, W. Cao, Q. Zhang, and P. Lu, Phys. Rev. Lett. **124**, 157403 (2020).

[21] Y.-T. Zhao, S.-Y. Ma, S.-C. Jiang, Y.-J. Yang, X. Zhao, and J.-G. Chen, Opt. Express **27**, 34392 (2019).

[22] K. Uchida, V. Pareek, K. Nagai, K. M. Dani, and K. Tanaka, Phys. Rev. B **103**, L161406 (2021).

[23] V.-H. Hoang and A.-T. Le, Phys. Rev. A **102**, 023112 (2020).

[24] T. T. Luu and H. J. Wörner, Nat. Commun. **9**, 916 (2018).

[25] A. A. Lanin, E. A. Stepanov, A. B. Fedotov, and A. M. Zheltikov, Optica **4**, 516 (2017).

[26] Y.-T. Zhao, X.-Q. Xu, S.-C. Jiang, X. Zhao, J.-G. Chen, and Y.-J. Yang, Phys. Rev. A **101**, 033413 (2020).

[27] A. McPherson, G. Gibson, H. Jara, U. Johann, T. S. Luk, I. A. McIntyre, K. Boyer, and C. K. Rhodes, J. Opt. Soc. Am. B **4**, 595 (1987).

[28] M. Ferray, A. L'Huillier, X. F. Li, L. A. Lompre, G. Mainfray, and C. Manus, J. Phys. B **21**, L31 (1988).

[29] G. Ndabashimiye, S. Ghimire, M. Wu, D. A. Browne, K. J. Schafer, M. B. Gaarde, and D. A. Reis, Nature (London) **534**, 520 (2016).

[30] X. Song, S. Yang, R. Zuo, T. Meier, and W. Yang, Phys. Rev. A **101**, 033410 (2020).

[31] F. Navarrete and U. Thumm, Phys. Rev. A **102**, 063123 (2020).

[32] I. Kilen, M. Kolesik, J. Hader, J. V. Moloney, U. Huttner, M. K. Hagen, and S. W. Koch, Phys. Rev. Lett. **125**, 083901 (2020).

[33] S. Jiang, J. Chen, H. Wei, C. Yu, R. Lu, and C. D. Lin, Phys. Rev. Lett. **120**, 253201 (2018).

[34] L. Yue and M. B. Gaarde, Phys. Rev. Lett. **124**, 153204 (2020).

[35] Y. S. You, M. Wu, Y. Yin, A. Chew, X. Ren, S. Gholam-Mirzaei, D. A. Browne, M. Chini, Z. Chang, K. J. Schafer, M. B. Gaarde, and S. Ghimire, Opt. Lett. **42**, 1816 (2017).

[36] J. Chen, M. Liu, X. Liu, Y. Ouyang, W. Liu, and Z. Wei, Nanophotonics **9**, 2549 (2020).

[37] Y. Feng, S. Shi, J. Li, Y. Ren, X. Zhang, J. Chen, and H. Du, Phys. Rev. A **104**, 043525 (2021).

[38] F. Li, N. Li, P. Liu, and Z. Wang, Opt. Express **30**, 10280 (2022).

[39] N. Tancogne-Dejean, O. Mücke, F. Kärtner, and A. Rubio, Nat. Commun. **8**, 745 (2017).

[40] Y. Lang, Z. Peng, and Z. Zhao, Chin. Phys. Lett. **39**, 114201 (2022).

[41] Y. Qiao, Y. Huo, H. Liang, J. Chen, W. Liu, Y. Yang, and S. Jiang, Phys. Rev. B **107**, 075201 (2023).

[42] Q. Peng, Z. Peng, Y. Lang, Y. Zhu, D. Zhang, Z. Lü, and Z. Zhao, Chin. Phys. Lett. **39**, 053301 (2022).

[43] G. Vampa, C. R. McDonald, G. Orlando, P. B. Corkum, and T. Brabec, Phys. Rev. B **91**, 064302 (2015).

[44] H. Liu, Y. Li, Y. S. You, S. Ghimire, T. F. Heinz, and D. A. Reis, Nat. Phys. **13**, 262 (2017).

[45] L. Yue and M. B. Gaarde, J. Opt. Soc. Am. B **39**, 535 (2022).

[46] D. Golde, T. Meier, and S. W. Koch, Phys. Rev. B **77**, 075330 (2008).

[47] G. Vampa, C. R. McDonald, G. Orlando, D. D. Klug, P. B. Corkum, and T. Brabec, Phys. Rev. Lett. **113**, 073901 (2014).

[48] M. Wu, S. Ghimire, D. A. Reis, K. J. Schafer, and M. B. Gaarde, Phys. Rev. A **91**, 043839 (2015).

[49] X.-Q. Wang, Y. Xu, X.-H. Huang, and X.-B. Bian, Phys. Rev. A **98**, 023427 (2018).

[50] Y.-T. Zhao, S.-C. Jiang, X. Zhao, J.-G. Chen, and Y.-J. Yang, Opt. Lett. **45**, 2874 (2020).

[51] T.-Y. Du, D. Tang, X.-H. Huang, and X.-B. Bian, Phys. Rev. A **97**, 043413 (2018).

[52] C.-L. Xia, Q.-Q. Li, Y.-Y. Lan, and X.-Y. Miao, Opt. Commun. **456**, 124626 (2020).

[53] T. Meier, G. von Plessen, P. Thomas, and S. W. Koch, Phys. Rev. Lett. **73**, 902 (1994).

[54] Y. Qiao, Y.-Q. Huo, S.-C. Jiang, Y.-J. Yang, and J.-G. Chen, Opt. Express **30**, 9971 (2022).

[55] S. Jiang, H. Wei, J. Chen, C. Yu, R. Lu, and C. D. Lin, Phys. Rev. A **96**, 053850 (2017).

[56] S. Jiang, C. Yu, J. Chen, Y. Huang, R. Lu, and C. D. Lin, Phys. Rev. B **102**, 155201 (2020).

[57] C. Altucci, V. Tosa, and R. Velotta, Phys. Rev. A **75**, 061401(R) (2007).

[58] C. Altucci, R. Velotta, V. Tosa, P. Villoresi, F. Frassetto, L. Poletto, C. Vozzi, F. Calegari, M. Negro, S. D. Silvestri, and S. Stagira, Opt. Lett. **35**, 2798 (2010).